European Journal of Control (1996) 2:166–175

European Journal of Control

On the Design and Implementation of a Rotary Crane Controller

Thomas Gustafsson

Control Engineering Group, University of Luleå, Luleå, Sweden

This paper deals with the feedback control of a rotary crane. The goal is to design a control system that assists the operator to move the cargo without oscillations and correctly align the cargo at the final position. This is accomplished with a weakly coupled pair of state feedback controllers with a nonlinear compensator. The controller has been implemented and tested on a real crane.

Keywords: Rotary crane; Pole placement control; Feedforward; State feedback; Speed control

1. Introduction

Rotary cranes are widely used as deck cranes on cargo vessels, usually manually operated by local harbor operators with different skill levels. Therefore, it is desirable to facilitate the crane operation for reasons of economy and safety of the operation. A complete automation of these types of cranes is difficult as it would require information on where to load and unload the cargo, a task that is usually performed by the operator. In [1,2] such an approach is taken where initial and terminal conditions are given and an optimal controller is used to make the transfer. Our approach is to keep the operator but let him control the motion of the cargo instead of controlling the crane motors. This can be realized by a linear feedback changing the dynamics in order to assist the operator.

It is a well-known fact that global non linear techniques can be used to deal with the problem of controlling nonlinear systems [3–5], this is especially true if the dynamics can be described by Euler–Lagrangian equations of motion, thus the rotary crane is a good candidate for global nonlinear control, these techniques are not used in this paper but it would certainly be valuable to compare the achievable performance with the performance of the controller presented in this paper.

The paper is organized as follows. In Section 2 we establish a dynamic model for a rotary crane with a point mass suspended with a wire. The section is logically divided into five parts. In the first part, the general case, there are no restrictions on the movements of the suspension point. In the second part treating the rotary crane case it is more natural to use the two crane angles θ and γ defined in Fig. 2 (later) as inputs. In the third part efforts are made to reduce the model complexity. Then the steady state behavior is discussed. In Section 3 the control design is outlined and Section 4 deals with leaning cranes. In Section 5 an implementation of the controller is tested on a real crane.

2. Dynamic Model

We consider the rotary crane shown in Fig. 1, where the boom angle γ is controlled by a wire which is wound around a drum. The body of the crane can be rotated about the z-axis by a rotation motor. The pivot of the boom does not necessarily coincide with the origin. To make it simple we regard the crane as a rigid body, and the load as a point mass. Further, we neglect frictional torques in the mechanism. The most crucial assumption is to neglect the dynamic influence of the load on the crane. This can be justified by a

Correspondence and offprint requests to: T. Gustafsson, Control Engineering Group, University of Luleå, S-971 87 Luleå, Sweden. E-mail: thomas@sm.luth.se

Received 17 January 1995; Accepted in revised form 24 June 1996
Recommended by C. Samson and D.W. Clarke

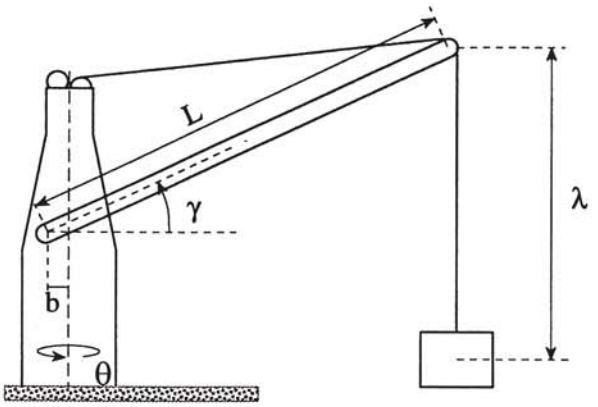

Fig. 1. Notations for a rotary crane, defining the angles θ and γ, the boom length L and the pivot offset b.

stiff crane machinery, which is the case for the cranes considered in this paper. For a leaning crane, it is, however, necessary to take into account how the load is influencing the crane.

The result of these assumptions is that the process can be described with three models, one each for the boom and rotation dynamics and one model for a two-dimensional pendulum driven by a three-dimensional acceleration defined in the suspension point.

2.1. General Case

In an inertial frame where $\chi_t = \{x_t, y_t, z_t\}$ are the coordinates of the suspension point and $\chi_m = \{x_m, y_m, z_m\}$ are the coordinates of the load, define the angle β as a positive rotation around the X-axis and α as a positive rotation around the Y-axis. The notation is used to emphasize that the second rotation, as illustrated in Fig. 2, is in the new frame defined by the first rotation. Such a set of rotation

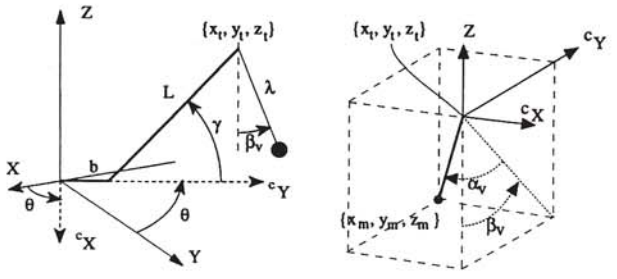

Fig. 2. Notations for a rotary crane. The left part shows the boom, defining the angles θ and γ, the boom length L, the length of the wire λ and the pivot offset b. The right part shows the load and the suspension point defining the load swing angles α and β. The coordinate axes without index is the inertial system. The crane-fixed system has index 'c'.

angles is called Euler angles [6] and gives the following expression for the coordinates of the load

$$\chi_m = \chi_t + \lambda \begin{pmatrix} -\sin\alpha \\ \cos\alpha\sin\beta \\ -\cos\alpha\cos\beta \end{pmatrix} \triangleq \chi_t + \lambda\Omega \qquad (1)$$

where λ is the length of the suspension wire. Using α and β as generalized coordinates we can use Euler–Lagrange equations [7] to establish a dynamic model. The kinetic and potential energies are

$$T = \frac{1}{2}m(\dot{x}_m^2 + \dot{y}_m^2 + \dot{z}_m^2) \qquad (2)$$

$$U = mgz_m \qquad (3)$$

where m is the mass of the load. With the Lagrangian as $\mathcal{L} = T - U$ we use Lagrange's equations

$$\frac{d}{dt}\left(\frac{\partial \mathcal{L}}{\partial \dot{q}_i}\right) - \frac{\partial \mathcal{L}}{\partial q_i} = 0 \qquad (4)$$

where q_i stands for the generalized coordinates α and β. A detailed derivation of the dynamics is found in [8] where (4) is solved for $\ddot{\alpha}$ and $\ddot{\beta}$ to give a coupled pair of second order differential equations

$$\lambda\ddot{\alpha} = \ddot{x}_t\cos\alpha - (g + \ddot{z}_t)\sin\alpha\cos\beta - 2\dot{\lambda}\dot{\alpha} + \ddot{y}_t\sin\alpha\sin\beta - \lambda\dot{\beta}^2\sin\alpha\cos\alpha \qquad (5a)$$

$$\lambda\cos\alpha\ddot{\beta} = -\ddot{y}_t\cos\beta - (g + \ddot{z}_t)\sin\beta - 2\dot{\lambda}\dot{\beta}\cos\alpha + 2\lambda\dot{\alpha}\dot{\beta}\sin\alpha \qquad (5b)$$

2.2. Rotary Crane Case

Since we are considering a rotary crane the natural choice of inputs are the crane rotation angle θ and the crane boom angle γ. From Fig. 2 we can derive that

$$\begin{aligned} x_t &= -(b + L\cos\gamma)\sin\theta \\ y_t &= (b + L\cos\gamma)\cos\theta \\ z_t &= L\sin\gamma \end{aligned} \qquad (6)$$

In order to achieve decoupling we define a crane-fixed frame, indicated in Fig. 2 by ${}^cX$ and ${}^cY$, that rotates with the crane such that the crane boom always coincides with the ${}^cY$-axis. The relation between a point in the inertial frame χ and the crane-fixed frame ${}^c\chi$ is then by definition

$$\chi = \begin{pmatrix} \cos\theta & -\sin\theta & 0 \\ \sin\theta & \cos\theta & 0 \\ 0 & 0 & 1 \end{pmatrix} {}^c\chi \triangleq {}_cR\,{}^c\chi \qquad (7)$$

Define the new Euler angles α_v and β_v, in the crane-fixed system such that the coordinate of the load is

$$ {}^{c}\chi_m = {}^{c}\chi_t + \lambda \begin{pmatrix} -\sin\alpha_v \\ \cos\alpha_v \sin\beta_v \\ -\cos\alpha_v \cos\beta_v \end{pmatrix} \triangleq {}^{c}\chi_t + \lambda\Omega_v \tag{8} $$

Inserting the last parts of (1) and (8) in the relation between coordinates in the inertial and crane-fixed system defined in (7) gives

$$ \chi_t + \lambda\Omega = {}_cR({}^{c}\chi_t + \lambda\Omega_v) = \chi_t + {}_cR\lambda\Omega_v \tag{9} $$

which simplifies to $\Omega = {}_cR\Omega_v$.

Now using $\chi_m = \chi_t + {}_cR\lambda\Omega_v$ when solving the Euler–Lagrange equations (2)–(4) gives the following equations of motion expressed in the crane-fixed load swing angles

$$ \begin{aligned} &\lambda\ddot{\alpha}_v = \\ &-g\sin\alpha_v\cos\beta_v - 2\dot{\lambda}\dot{\alpha}_v - \lambda\dot{\beta}_v^2\sin\alpha_v\cos\alpha_v \\ &\quad + L\sin\alpha_v\sin(\gamma-\beta_v)\,\dot{\gamma}^2 \\ &\quad - (2\dot{\lambda}\sin\beta_v + 2\lambda\dot{\beta}_v\cos^2\alpha_v\cos\beta_v)\,\dot{\theta} \\ &\quad + 2L\dot{\gamma}\dot{\theta}\cos\alpha_v\sin\gamma \\ &\quad + (\lambda\cos\alpha_v\cos^2\beta_v - (b+L\cos\gamma) \\ &\qquad \sin\beta_v)\,\dot{\theta}^2\sin\alpha_v \\ &\quad - L\sin\alpha_v\cos(\gamma-\beta_v)\,\ddot{\gamma} \\ &\quad - (\lambda\sin\beta_v + (b+L\cos\gamma)\cos\alpha_v)\,\ddot{\theta} \end{aligned} \tag{10a} $$

$$ \begin{aligned} &\lambda\ddot{\beta}_v\cos\alpha_v = \\ &-g\sin\beta_v + 2\lambda\dot{\alpha}_v\dot{\beta}_v\sin\alpha_v \\ &+ L\cos(\gamma-\beta_v)\,\dot{\gamma}^2 - 2\dot{\lambda}\dot{\beta}_v\cos\alpha_v \\ &+ 2(\lambda\dot{\alpha}_v\cos\alpha_v + \dot{\lambda}\sin\alpha_v)\,\dot{\theta}\cos\beta_v \\ &+ (\lambda\cos\alpha_v\sin\beta_v + b + L\cos\gamma)\,\dot{\theta}^2\cos\beta_v \\ &+ L\sin(\gamma-\beta_v)\,\ddot{\gamma} + \lambda\sin\alpha_v\cos\beta_v\,\ddot{\theta} \end{aligned} \tag{10b} $$

The derivation of the equations above is with advantage performed with a symbol manipulation program.

2.3. Steady State

The steady state solution of the nonlinear model (10) is obtained by inserting the solution $\bar{\alpha}_v = 0$ from (10a) into (10b) giving

$$ 0 = -g\sin\beta_v + (\lambda\sin\beta_v + b + L\cos\gamma)\dot{\theta}^2\cos\beta_v \tag{11} $$

This can be rewritten as a quartic equation in $s \triangleq \sin\beta_v$

$$ a^2s^2 + (s^2-1)(s+x)^2 = 0 \tag{12} $$

where $a = \omega^2/\dot{\theta}^2$ and $x = (b + L\cos\gamma)/\lambda$. The explicit solution of (12) is rather voluminous and we confine ourselves to merely stating that $\bar{\beta}_v$ can be approximated by

$$ \sin\bar{\beta}_v \approx \frac{b + L\cos\gamma}{g - \lambda\dot{\theta}^2}\dot{\theta}^2 \tag{13} $$

3. Control Design

The objective of this section is to design a servo controller that facilitates, not automates, the use of a rotary crane. This distinction is very important to make, since the operator remains as an integrated and commanding part in our approach.

The operator is responsible for the overhead strategy, where to load and where to unload. He should also take necessary actions to operate the control levers to move the crane, and the load, into appropriate positions. Moving the load is the difficult part since it calls for a high degree of skill and concentration to avoid unnecessary time delays due to oscillation of the crane load.

The idea with a facilitating servo is to remove the tricky dynamics and let the angular rate of the load be directly proportional to the angles of the control levers. This is unfortunately not possible due to limitations in the crane machinery. But it should be possible to let the load behave as a well damped linear system.

This obviously leads to a need for mental adaptation by the operator. He should now ignore the movements of the crane and concentrate on the load. In a study by Schmidtbauer and Rönnbäck [9] it is, however, shown that well-damped process dynamics, in contrast to undamped dynamics, reduce both the learning time and the cycle time even for an untrained operator.

A reason to use a rate servo controller instead of a position controller is that it is important to have a simple man–machine interface. Rotary cranes used on ships are usually operated by local dock workers. It is thus not possible in practice to train an operator on a crane with complex or different man–machine interface.

3.1. Linear Design

Before considering a full-blown controller, let us step back and start by considering the linearized versions of the equations of motion for a pendulum in a crane-fixed frame (10)

$$\ddot{\alpha}_v = -\omega^2 \alpha_v - L_\alpha \ddot{\theta} \tag{14a}$$

$$\ddot{\beta}_v = -\omega^2 \beta_v + L_\beta \ddot{\gamma} \tag{14b}$$

where

$$\omega^2 \approx g/\lambda$$

$$L_\alpha = \frac{b + L\cos\gamma}{\lambda}$$

$$L_\beta = \frac{L\sin\gamma}{\lambda} \tag{15}$$

Thus we simplify the controller design as we can decompose the controller into two parts and treat them separately. One purpose with this is to show that it is necessary to take the cross-coupling into consideration.

We also need linear models of the crane. If we ignore or assume that we can compensate time delay and nonlinearities in the actuators, then we can model them as linear first order systems (see [8]).

$$\ddot{\theta} = k_\theta(u_\theta - \dot{\theta}) \tag{16a}$$

$$\ddot{\gamma} = k_\gamma(u_\gamma - \dot{\gamma}) \tag{16b}$$

where u_θ and u_γ are inputs to the actuators.

Since the linear models of the slewing motion and the luffing motion have identical structure, and differ only in the values of the parameters, it is at this stage only necessary to study one of them. Our choice is to study the slewing motion.

3.2. Linear Control of the Slewing Motion

Having linear models of both the load and the crane we can combine them into a fourth order state space model for the rotational or slewing movement. The natural choice of state vector is $x = (\alpha_v \quad \dot{\alpha}_v \quad \theta \quad \dot{\theta})^T$ which gives the linear state space description $\dot{x} = \mathcal{A}x + \mathcal{B}u_\theta$ where

$$\mathcal{A} = \begin{pmatrix} 0 & 1 & 0 & 0 \\ -\omega^2 & 0 & 0 & L_\alpha k_\theta \\ 0 & 0 & 0 & 1 \\ 0 & 0 & 0 & -k_\theta \end{pmatrix} \qquad \mathcal{B} = \begin{pmatrix} 0 \\ -L_\alpha k_\theta \\ 0 \\ k_\theta \end{pmatrix} \tag{17}$$

The goal with the controller, as mentioned before in this section, is to make it easier for the operator to handle the crane. Originally, in a manual system, the slewing motion of the crane is controlled by an operator with a control stick, where the slew rate of the crane is proportional to the stick angle. The problem with the manual mode is that the operator has to compensate for the undamped oscillation modes in the dynamics of the load. To avoid this, a controller can be used to automatically stabilize the pendulum motion.

Furthermore, to avoid confusion, it is necessary to redefine the control stick function. Instead of being proportional to the crane slew rate the control stick angle should be proportional to the speed or angular rate of the load orthogonally to the crane arm. This speed can be calculated by taking the scalar product between a direction vector orthogonal to the crane arm and the velocity vector of the load. Then normalize with the radius to get the angular rate. The coordinates of the load in the crane fixed frame are $\{{}^c x_m, {}^c y_m\}$ and the direction orthogonal to the crane arm is $\{-1, 0\}$ which gives angular rate of the load as

$$y(t) = \dot{\theta} - \frac{{}^c\dot{x}_m}{\sqrt{{}^c x_m^2 + {}^c y_m^2}} \tag{18}$$

where a term $\dot{\theta}$ is added since the crane fixed frame is rotating with that rate. The radius can be approximated with

$$\sqrt{{}^c x_m^2 + {}^c y_m^2} \approx {}^c y_m \approx b + L\cos\gamma = \lambda L_\alpha \tag{19}$$

Using a small angle approximation and assuming constant wire length λ then ${}^c\dot{x}_m = -\lambda\dot{\alpha}_v$ which together with (17) inserted in (16) gives

$$y = \dot{\theta} + \frac{1}{L_\alpha}\dot{\alpha}_v \tag{20}$$

The open loop transfer function from the input u_θ to the angular rate y of the load is

$$\frac{Y(s)}{U_\theta(s)} = \frac{k_\theta s}{s(s + k_\theta)} - \frac{k_\theta s^2}{(s + k_\theta)(s^2 + w^2)} \tag{21}$$

where $Y(s)$ and $U_\theta(s)$ are the Laplace transforms of the angular rate $y(t)$ and u_θ, the control signal defined in (16a).

Now our goal is to design a state space controller

$$u_\theta = Gv(t) - Kx(t) \tag{22}$$

such that the angular rate of the load $y(t)$ as well as possible tracks the demanded angular rate $v(t)$. Since $\{\mathcal{A}, \mathcal{B}\}$ forms a controllable pair it is possible to design a linear state controller, such as (22), and arbitrary place the closed loop poles. The open system (21) has poles in 0, $-k_\theta$ and $\pm j\omega$. It is reasonable not to modify the two real poles which originate from the crane dynamics. The poles on the imaginary axis must, however, be modified to have negative real parts. A standard state space pole placement method [10] can be used and straightforward calculations show that the control law

$$u_\theta = \frac{\omega_c^2}{\omega^2} v(t) - k_1^\alpha \alpha_v - k_2^\alpha \dot{\alpha}_v - k_4^\alpha \dot{\theta} \tag{22}$$

with the gains

$$k_1^\alpha = -\frac{2\xi\omega_c}{L_\alpha} - \frac{\omega_c^2 - \omega^2}{k_\theta L_\alpha}$$
$$k_2^\alpha = -\frac{2\xi\omega_c}{k_\theta L_\alpha} + \frac{\omega_c^2 - \omega^2}{L_\alpha \omega^2}$$
$$k_4^\alpha = \frac{\omega_c^2 - \omega^2}{\omega^2} \tag{24}$$

gives the closed loop transfer function

$$\frac{Y(s)}{U_\theta(s)} = \frac{k_\theta \omega_c^2}{(s + k_\theta)(s^2 + 2\xi\omega_c s + \omega_c^2)} \tag{25}$$

In Fig. 3 we can see the result of a simulation of the closed loop system for a typical crane. It shows an evident coupling between the systems (14a) and (14b) with oscillations in β_v initiated by the rotation, but it also shows that a linear controller like (23) can be used to eliminate the oscillations orthogonal to the crane arm.

In an effort to maintain a good man–machine interface the next step is to modify (23) to avoid oscillations in β_v. The reason for calling it a man–machine interface is that if the operator initiates a slewing motion with the control stick then the luffing motion should be kept to a minimum.

3.3. Linear Control of the Luffing Motion

This is an easier task than controlling the slewing motion since a change of the luffing angle γ does not affect the slewing angle α_v. Both the linearized dynamics and the objectives of the control are equal to that of the slewing motion. Thus we can use the same controller structure as in Section 3.2.

$$u_\gamma = \frac{\omega_c^2}{\omega^2} v_\gamma - k_1^\beta \beta_v - k_2^\beta \dot{\beta}_v - k_4^\beta \dot{\gamma} \tag{26}$$

where we prudently remember the sign difference in (24) when the controller gains are calculated

$$k_1^\beta = \frac{2\xi\omega_c}{L_\beta} + \frac{\omega_c^2 - \omega^2}{k_\gamma L_\beta}$$
$$k_2^\beta = \frac{2\xi\omega_c}{k_\gamma L_\beta} - \frac{\omega_c^2 - \omega^2}{L_\beta \omega^2}$$
$$k_4^\beta = \frac{\omega_c^2 - \omega^2}{\omega^2} \tag{27}$$

to get the closed loop poles 0, $-k_\theta$ and a double pole in $-\omega_c$.

A crucial difference from the slewing controller is that the crane arm angle γ is typically limited to angles between 15° and 80° and the controller has to stop before the limits to avoid the oscillations resulting from a quick stop. In Fig. 4 we can also note that the system is not critically damped as expected, probably because the parameter L_β varies with the crane arm angle γ.

3.4. Simultaneous Control of Slewing and Luffing

Some progress has now been made towards the construction of a linear controller, but as noted in Section 3.2 it still remains to solve the problem arising from the coupling between the systems. Notice in Fig. 3 that a step in the set point for the slew rate excites an oscillation in β_v, furthermore notice that the load swing angle β_v is biased. All efforts to eliminate the bias will undoubtedly lead to a system with constantly decreasing crane arm angle γ in the effort to compensate the load swing angle caused by the centrifugal force. Consequently we should only try to eliminate the oscillation allowing the bias to exist. A straightforward method is to use the stationary solution (13) of (10) as an approximation of the bias and modify (26) to

$$u_\gamma = v_\gamma - k_1^\beta(\beta_v - \bar{\beta}_v) - k_2^\beta \dot{\beta}_v - k_4^\beta \dot{\gamma} \tag{28}$$

where the gains are the same as in (27).

Simulating the same typical crane as in Fig. 3 with the modified control law (28) together with the slew-

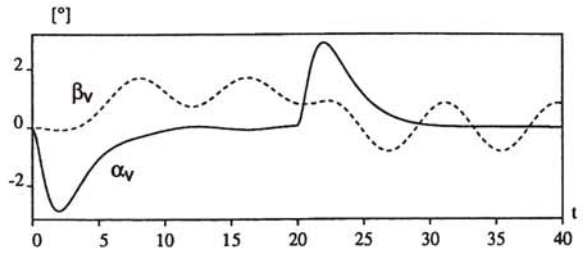

Fig. 3. Simulation of the linear state space controller (23) with $\omega_c = \omega = 0.7381$ and $\xi = 1$ that among other things shows that the decoupled models (14a) and (14b) should be coupled.

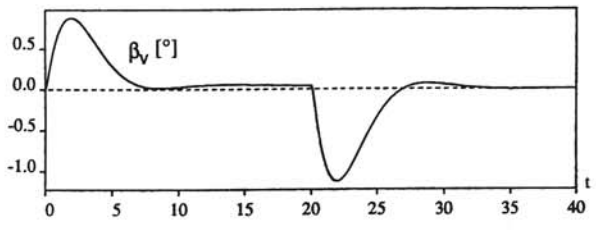

Fig. 4. Simulation of the linear state space controller (26) with $\omega_c = \omega = 0.7381$ and $\xi = 1$. The reference value to the controller $v_\gamma = 0.5\dot{\gamma}_{max}$ during the first 20 s of the simulation and then set to zero.

ing motion controller (23) shows a pronounced improvement, not only for β_v but also for α_v. In the latter case it is mainly because the system eventually reaches a steady state where $\dot{\beta}_v = 0$ which, according to (10) reduces the coupling. The result of the simulation is displayed in Fig. 5.

A remaining problem with the controller (28) is conspicuous if we study the variation of γ in Fig. 6 from the same simulation as in Fig. 5. Despite the fact that only the set point for the slew rate has been changed there is an unwanted steady-state error in the luffing angle γ.

The reason for this is that the closed loop system has a pole in the origin and a disturbance not balanced by a comparable disturbance with opposite sign will leave a trace in γ. Thus one solution to the problem is to change the pole placement of the luffing controller such that the closed loop transfer function from the reference value v_γ to the crane arm angle γ becomes

$$\frac{\Gamma(s)}{V_\gamma(s)} = \frac{pk_\gamma\omega_c^2}{(s+p)(s+k_\gamma)(s^2+2\xi\omega_c s+\omega_c^2)} \tag{29}$$

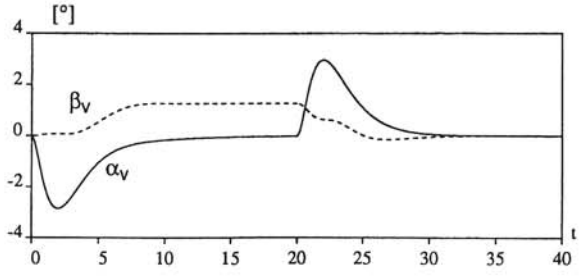

Fig. 5. Simulation of the nonlinear controller (28). The reference value to the controller $v_\theta = 0.8\dot{\theta}_{max}$ during the first 20 s of the simulation and then set to zero. Notice that, in contrast to Fig. 3, there are no overshoots in α_v.

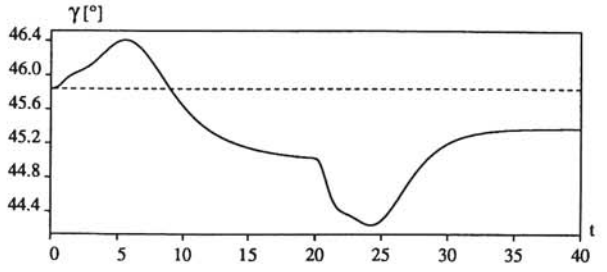

Fig. 6. Simulation of the controller (28). The reference value to the controller $v_\theta = 0.8\dot{\theta}_{\max}$ during the first 20 s of the simulation and then set to zero. Note that γ changes despite the fact that only the slew rate set point has been changed.

The control law (28) should then be modified to

$$u_\gamma = k_3^\beta v_\gamma - k_1^\beta(\beta_v - \bar{\beta}_v) - k_2^\beta\dot{\beta}_v - k_3^\beta\gamma - k_4^\beta\dot{\gamma} \tag{30}$$

where for the special case when $\omega_c = \omega$

$$k_1^\beta = \frac{2\xi_\beta\omega(k_\gamma+p)}{k_\gamma L_\beta} \qquad k_2^\beta = -\frac{2\xi_\beta(\omega^2-k_\gamma p)}{L_\beta k_\gamma\omega}$$

$$k_3^\beta = p \qquad k_4^\beta = p\left(\frac{1}{k_\gamma}+2\xi_\beta\omega\right)$$

The effect of this modification can clearly be seen in Fig. 7.

The use of a position controller for the luffing motion also solves the problem mentioned at the end of Section 3.2, that arises from the limitations of the crane arm angle γ. A well-behaved closed loop system (29) with a damping ratio $\xi = 1$ has no overshoot in γ, so it is safe to give a set point to (30) that is close or equal to a limit. To make the closed loop system behave like a rate controller it is necessary to integrate the rate set point from the command stick to obtain an appropriate position set point.

4. Leaning Cranes

This section treats the common case when the rotary crane is mounted on a cargo vessel with an inclination. The slope of the vessel has two essential effects on the control system. Principally, the measurement system must be enhanced to be able to correctly measure the angles α_v and β_v even if the ship, and with it the crane, is leaning. For a while we consider this enhancement as done and trust the measurements. In [8] it is shown how to enhance the measurement system.

The second effect is that the load will influence a leaning crane with a static torque which can be devastating especially in cranes with hydraulic motors. The

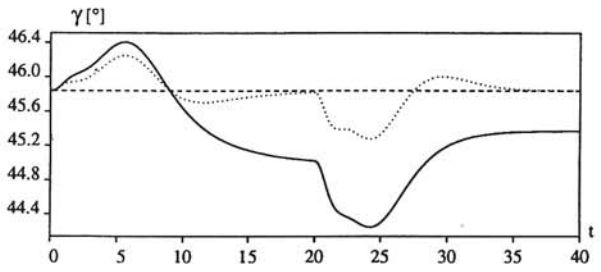

Fig. 7. Simulation showing the improved decoupling with the position controller (30) compared to the rate controller (28). The solid curve is the same as in Fig. 6. The reference value $v_\theta = 0.8\dot{\theta}_{\max}$ during the first 20 s of the simulation and then set to zero.

problem is most pregnant when both the crane and the load are at rest, since a hydraulic motor may be stiff towards dynamic loads, but when it comes to static loads there is always a leak flow in the motor that causes the motor and consequently the crane to move. The normal way to solve this in a manually operated crane is to use a mechanical brake that automatically switches on when the motor is supposed to be at rest.

Mechanical brakes are, however, unacceptable, or at least difficult, to use in an automatic system, since they are slow in action and thus introduce time delays that can be difficult to handle. Only when loading or unloading should the brakes be used to increase the security.

Apparently a modification of the controller is necessary to avoid sliding cranes. A first step is to model the disturbance by modifying (16a) to

$$\ddot{\theta} = k_\theta(u_\theta - \dot{\theta}) + \delta(t) \tag{31}$$

where we in a first attempt consider $\delta(t)$ as constant. If this was true then an integrating controller would solve our problem. But unfortunately it is not true unless θ is constant, as a strict analysis shows that $\delta(t)$ is dependent on θ according to

$$\begin{aligned}\delta(t) &= \mu Mgr \\ &= \mu Mg(b + L\cos\gamma)(\sin\zeta_r\cos\theta \\ &\quad - \cos\zeta_r\sin\zeta_p\sin\theta)\end{aligned} \tag{32}$$

where r is the momentum arm. The mass of the load is denoted by M and the roll and pitch angles defined in Fig. 8 are denoted by ζ_r and ζ_p. Those three quantities are normally unknown. Even the coefficient μ is unknown. For the crane used in our experiments then $|\delta(t)| < 0.02$.

To make the analysis easier we exclude the small vessel case when a moving crane can change the slope of the vessel. Then all quantities in (32) except θ are constant and (32) can be reduced to

$$\delta(t) = \mu_1\cos\theta + \mu_2\sin\theta \tag{33}$$

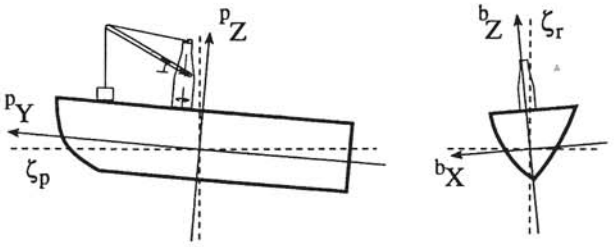

Fig. 8. Definition of roll angle ζ_r and pitch angle ζ_p. The crane arm is directed to the stem when $\theta = 0°$.

Linearization of (33) around θ_0 gives

$$\begin{aligned}\delta(t) &\approx \mu_1\cos\theta_0 + \mu_2\sin\theta_0 \\ &\quad + (\mu_2\cos\theta_0 - \mu_1\sin\theta_0)(\theta - \theta_0) \\ &= \delta_0 + \kappa_0\theta\end{aligned}$$

Thus if the variation in θ is sufficiently small then $\delta(t)$ can be considered as a constant disturbance to a slightly modified system. It may, however, not be possible to use this linearization since θ is subjected to large variations. Principally there are two different solutions:

- With knowledge of $\delta(t)$, then feedforward and gain scheduling can be used to compensate for leaning cranes.
- Without knowledge of $\delta(t)$ then the controller, in some sense, must be robust.

Regardless of the structure of the controller, it can not be the rate controller (23) since the closed loop system then has a pole in the origin. The Laplace transform of θ for the closed loop system controlled by (23) and with a constant disturbance $\delta(t)$ is

$$\Theta(s) = \frac{k_\theta\omega_c^2 V_\theta(s) + k_\theta\omega^2\Delta(s)}{s(s + k_\theta)(s^2 + 2\xi\omega_c s + \omega_c^2)} \tag{35}$$

A constant disturbance δ will thus make the angle θ drift away.

Redesigning (23) to a position controller similar to the one previously designed for the luffing motion gives an immediate improvement. The difference is displayed in Fig. 9. An important difference is that the position controller is slower than the rate controller. This is clearly noticeable sitting in the operator's cabin. The position controller feels viscous compared to the rate controller. Although the difference in time is small this viscous feeling leads an experienced operator to believe that the automatic controller is slow and inferior. The reason is of course the extra pole that is introduced with the position controller.

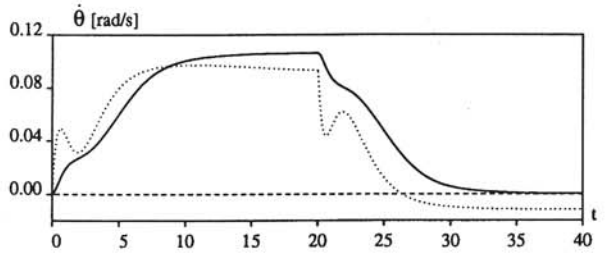

Fig. 9. Comparison of the slew rate $\dot{\theta}$ between a rate controller (dashed curve) and a position controller (solid curve). The crane is leaning $\zeta_p = -5°$. The rate controller gives a steady-state error causing the crane to glide away.

To improve the speed, this new pole can, however, be canceled by a set point filter

$$u_\theta = k_3^\alpha(\dot{v} + pv) - k_1^\alpha \alpha_v - k_2^\alpha \dot{\alpha}_v - k_3^\alpha \theta - k_4^\alpha \dot{\theta} \tag{36}$$

where v is the set point and p is the pole to cancel, the difference can be seen in Fig. 10. The same improvement in speed can also be made for the luffing controller by extending (30) with a set point filter.

Note that it is not necessary to base the control design on the dynamics for a leaning crane. The linear model (14), augmented with a term describing the centrifugal force, gives adequate precision provided that the slope angles of the crane are small and that the ratio between $\dot{\theta}$ and ω is sufficiently small.

In an effort to increase the quality of the man–machine interface we observe that the horizontal distance ${}^c y_m$ from a vertical axis, that coincides with the rotational axis of the crane at the rotary joint, to a load without oscillations can be calculated as

$${}^c y_m = (b + L\cos\gamma) - \zeta_\gamma L \sin\gamma \tag{37}$$

where $\zeta_\gamma = \zeta_r \sin\theta + \zeta_p \cos\theta$. Obviously the distance changes even if the crane arm angle γ is kept constant.

We stated in the previous section that if the operator only intends to rotate the crane, then it shall only rotate. We have, however, already made some exceptions from that rule as it is otherwise impossible to successfully eliminate the oscillations of the load.

The rule can also be interpreted as that the distance ${}^c y_m$, defined above, should be kept constant during a rotation. From (37) we conclude that the only way to accomplish this is to change γ with feedforward. Let γ_r be the set point due the operator. Then the set point to the controller γ_c is calculated from the equality

$$(b + L\cos\gamma_r) = (b + L\cos\gamma_c) - \zeta_\gamma L \sin\gamma_c \tag{38}$$

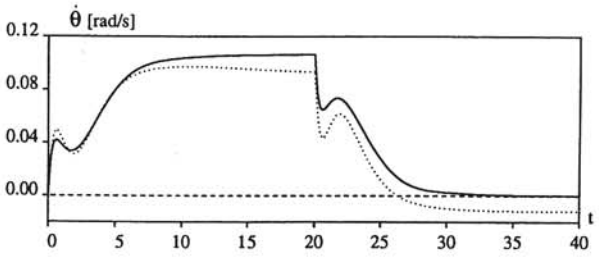

Fig. 10. Comparison of the slew rate $\dot{\theta}$ between a rate controller (dashed curve) and a position controller with set point filter (solid curve). The crane is leaning 5°. The rate controller gives a steady-state error causing the crane to glide away.

where the left part is the distance that the operator wants. Solving (38) gives the new set point

$$\cos\gamma_c = \frac{\cos\gamma_r + \zeta_\gamma\sqrt{\zeta_\gamma^2 + \sin^2\gamma_r}}{1 + \zeta_\gamma^2} \approx \cos\gamma_r + \zeta_\gamma \sin\gamma_r \tag{39}$$

To get the best tracking one should use the set point for slew angle θ, as in Fig. 11, to calculate ζ_γ when making the correction of the set point for the crane arm angle γ.

An additional feature with this procedure is that the suspension point will always follow a circular path when pure rotation is demanded thus decreasing the influence on the pendulum dynamics that a leaning crane has.

5. Full Scale Experiments

Experiments have been performed on a hydraulically powered rotary crane of type G-2 manufactured by AB Hägglund & Söner. The crane was mounted on their special test platform that made it possible to lean the crane. All results presented in this chapter come from experiments made when the crane was leaning with $\zeta_p = -5°$ and $\zeta_r = 0°$. See definition of the leaning angles in Fig. 8.

Some other features of the G-2 crane used in the experiments are:

- arm length $L = 27.085$ m
- maximal slewing speed $\dot{\theta}_{max} = 8\ °/s$
- maximal luffing speed $\dot{\gamma}_{max} = 2\ °/s$
- maximal hoisting speed $\dot{\lambda}_{max} = 0.5$ m/s
- length of wire $\lambda = 18$ m
- initial arm angle $\gamma = 50°$
- initial slew angle $\theta = 0°$

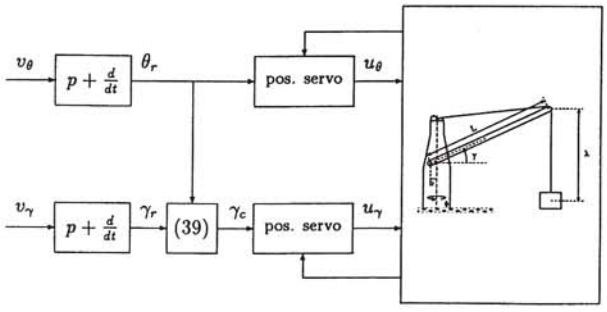

Fig. 11. The complete controller with feedforward from the slew angle command signal to the luffing angle set point. v_θ and v_γ are the command signals from the control sticks that serve as angular rate references. They are modified with a filter to position set points θ_r and γ_r. The control outputs are u_θ and u_γ.

- hoisting capacity 40 metric tonnes.
- weight of load $M = 8$ metric tonnes

The reason for using a rather upright arm was to have a wire length comparable to the lengths that are common in a real situation where the crane is mounted on a high pillar.

The hydraulic system of the crane was supplemented with electrical valves to allow remote control of the motors. Shaft encoders were used to measure both the slew angle θ and the arm angle γ. A mechanical sensor was used to measure the load swing angles α_v and β_v. There was no easy way to measure the wire length, but the crane has a construction that keeps the load at a constant height with varying arm angles. If the wire length is known for one arm angle, then it is easy to calculate the actual wire length, provided there is no hoisting.

A predecessor of RegSim [11] was used to implement an extended Kalman filter and the control law described in Section 3 along with a complete set of simulation models. The advantage of using the same implementation of the controller in simulation and in control of the real process was considerable, since the sources of obnoxious behavior could easily be traced down by comparing the simulation with the real world appearance.

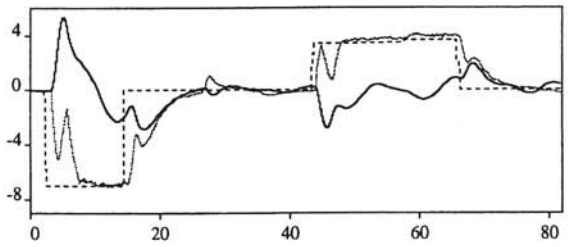

Fig. 12. Control experiment with the slewing motion controller. The solid curve is the load swing angle α_v, the dashed curve is the command signal v_θ and the dotted curve is the slew rate $\dot{\theta}$.

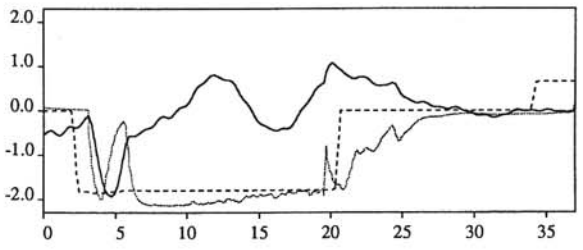

Fig. 13. Control experiment with the crane arm controller. The solid curve is the load swing angle β_v, the dashed curve is the command signal v_γ and the dotted curve is the crane arm angular rate $\dot{\gamma}$.

5.1. Control Experiments

Early experiments showed that the time delays in the motor drives were of such a magnitude that they could not be ignored in the control design. But with the Kalman filter as a base a prediction was made of all state variables used in the controller and no modification to the controller was necessary beyond that. The controller was implemented in two subsystems with different sampling periods. In the fastest system with a sampling period of 4 ms necessary measurements and digital filtering were made. The observer and the controller had a sampling period of 0.2 s.

Unfortunately there are very few appropriate experiment results that are saved. Most of the experiments results that are saved were made mainly to verify the function of the measurement and observer system since it turned out that this was the weak point in the system. The problems we had were mainly due to the low resolution in the 8-bit A/D-converters that we were using.

A direct comparison of the angular rate $\dot{\theta}$ in Figs 10 and 12 reveals, among other things, that the real crane has a higher acceleration than the simulated crane. We can, however, from Figs 12–14 see that the overall behaviour is still the same. A typical transition, from a steady state without oscillations, starts with a short acceleration phase of the crane. The load is almost at rest during this phase. Thus the load swing angle originates mainly from movement of the crane. In the next phase the angular rate of the crane is decreased until the load gains momentum and reaches the same speed as the crane. Then the crane accelerates to the desired oscillation free speed.

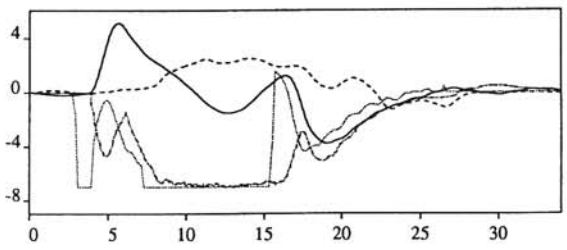

Fig. 14. Control experiment with both controllers. The solid and dashed curves show the load swing angles α_v and β_v.The dotted curve is the command signal u_θ and the dot-dashed curve shows the slew rate $\dot{\theta}$. The oscillations in β_v mainly originate from the wire-hook system.

6. Conclusions

In this paper we have discussed a method to design linear gain scheduled controllers for both the slew and luffing motion of a rotary crane. It is shown that the coupling between the slew and luffing motion can be eliminated with a nonlinear feedforward term. Further it is shown that the case with a leaning crane can be handled with a different choice of parameters in the controller.

The results given above have been confirmed in practice and a slightly different controller has been commercialized and is sold under the name 'Swing Defeater'.

Acknowledgements

This work has been partially supported by the Swedish National Board for Technical Development under contract 83-3039 and by AB Hägglunds & Söner.

References

1. Sakawa Y, Nakazumi A. Modeling and control of a rotary crane. ASME J of Dyn Syst, Measurement, and Con 1985; 107: 200–206
2. Sakawa Y, Shindo Y, Hashimoto Y. Optimal control of a rotary crane. ASME Journal of Optimization Theory and Applications 1981; 35: 535–557
3. Isidori A. Nonlinear control systems. Springer-Verlag, Berlin 1989
4. Nijmeijer H, van der Schaft AJ. Nonlinear dynamical control systems. Springer-Verlag, New York 1990
5. Vidyasagar M. Nonlinear systems analysis. Prentice-Hall, Englewood Cliffs, NJ 1993
6. Craig JJ. Introduction to robotics: mechanics and control. Addison-Wesley, New York 1989
7. Landau LD, Lifshitz EM. Mechanics. vol 1. Pergamon Press, Oxford 1978
8. Gustafsson T. Modelling and control of rotary crane systems. Doctor of technology thesis, Luleå University, June 1993
9. Schmidtbauer B, Rönnbäck S. Computer assisted manual control of cargo handling with ship cranes. In: Proc of the First European annual conference on human decision making and manual control, May 1981 pp 287–296
10. Kailath T. Linear systems. Prentice-Hall, London 1980
11. Gustafsson T. RegSim: A software tool for real time control and simulation. In: Proc of 4th IEEE CCA, Albany, New York 1995